Philosophical Magazine

ISSN: 1478-6435 (Print) 1478-6443 (Online) Journal homepage: https://www.tandfonline.com/loi/tphm20

First-principles investigation of $LaGaO_3$ and $LaInO_3$ lanthanum perovskite oxides

Aytaç Erkişi, Gökhan Gökoğlu, Gökhan Sürücü, Recai Ellialtıoğlu & Erdem Kamil Yıldırım

To cite this article: Aytaç Erkişi, Gökhan Gökoğlu, Gökhan Sürücü, Recai Ellialtıoğlu & Erdem Kamil Yıldırım (2016) First-principles investigation of $LaGaO_3$ and $LaInO_3$ lanthanum perovskite oxides, Philosophical Magazine, 96:19, 2040-2058, DOI: 10.1080/14786435.2016.1189100

To link to this article: https://doi.org/10.1080/14786435.2016.1189100

PHILOSOPHICAL MAGAZINE, 2016
VOL. 96, NO. 19, 2040–2058
http://dx.doi.org/10.1080/14786435.2016.1189100

Taylor & Francis
Taylor & Francis Group

First-principles investigation of $LaGaO_3$ and $LaInO_3$ lanthanum perovskite oxides

Aytaç Erkişi[a], Gökhan Gökoğlu[b], Gökhan Sürücü[c,d], Recai Ellialtıoğlu[a] and Erdem Kamil Yıldırım[e]

[a]Department of Physics Engineering, Hacettepe University, Ankara, Turkey; [b]Department of Physics, Karabük University, Karabük, Turkey; [c]Department of Electrics and Energy, Ahi Evran University, Kırşehir, Turkey; [d]Photonics Application and Research Center, Gazi University, Ankara, Turkey; [e]Department of Computer Engineering, Kırıkkale University, Kırıkkale, Turkey

ABSTRACT

Among the class of ABO_3 type perovskite oxides, $LaMO_3$ (M=Ga and In) compounds are investigated in cubic (*Pm-3m*), tetragonal (*P4mm*), hexagonal (*P-3m1*), rhombohedral (*R-3c*), and orthorhombic (*Pbnm*) phases by using generalized gradient approximation (GGA) within the density functional theory. On-site Coulomb interaction is also included in the calculations (GGA + *U*). After the determination of the stable phase, phase transition pressures have been calculated also. Then, their full structural, mechanical, electronic, optical and vibrational properties have been studied in stable orthorhombic (*Pbnm*) phase. Both compounds are non-magnetic insulators in their ground states. The energy gaps (E_g) of $LaGaO_3$ and $LaInO_3$ compounds have been found as 3.14 and 2.55 eV, respectively. The calculated elastic constants and phonon dispersion curves confirm the stability of orthorhombic phase mechanically and dynamically.

ARTICLE HISTORY
Received 18 January 2016
Accepted 6 May 2016

KEYWORDS
Perovskites; *ab initio*; band calculations; elasticity; phonons

1. Introduction

The perovskite structure has a general formula of ABC_3. The perovskite oxide structure is obtained by placing oxygen at C- anion site. Usually, the A and B cations are alkali metals, alkaline earth metals, transition metals or rare earth elements. Oxygen anions construct an octahedron around B cations in ABO_3 type perovskite oxide structures. It is known that ideal perovskite structure is cubic which comforms to *Pm3m* space group. In cubic perovskites, A cation is located at the corners of the cube, B cation is in the center and oxygen ions in the face-centers. Also there are tetragonal, orthorhombic, rhombohedral, monoclinic, and triclinic perovskites which are formed by the distortion of the ideal cubic structure through tilting of the BO_6 octahedra [1]. Usually, this type of orthorhombic perovskites is named as $GdFeO_3$ type perovskites [2].

Perovskite oxide materials are able to exhibit insulator, metal, semiconductor or superconductor properties. There are delocalized energy bands in some cases or there are localized

CONTACT Aytaç Erkişi erkisi@hacettepe.edu.tr

electrons or some transitions between these two behaviors seen. Also, most of the perovskites are found to be in magnetic order [3]. Therefore, their physical and chemical behaviors such as the density of states (DOS), Fermi surface, dielectric function, and phonon dispersion have special character [4]. In addition, as stated above, they exhibit very different physical properties; such as conductivity, magnetism, dielectricity, photonics, piezoelectricity, pyroelectricity and so that they can be used in many applications in a wide area.

There are comprehensive studies in the literature on a large family of perovskites [4]. In that work, the perovskite structures with cations having s- and d-electrons in the outer orbit are presented. But, over the past few decades, perovskites having rare earth elements with f-electrons as cations are particularly the subject of experimental studies.

Until now, perovskites have been the subject for quite large and important applications such as photochromic [5, 6], electrochromic [7, 8] and energy storage [9, 10] devices. Also, the piezoelectric [11], ferroelectric [12], dielectric [13, 14] and pyroelectric [15] properties are used in devices for switching, filtering and surface acoustic wave signal processing. Many of them have catalytic activity [16] and are used extensively for oxidation of carbon monoxide and hydrocarbons [17, 18], reduction of nitrogen oxide [19, 20], to obtain hydrogen from water with photoelectrolysis [21, 22] and other solid-state electrolysis cells [23].

In this work, we chose $LaGaO_3$ and $LaInO_3$ perovskite oxides from the family of $GdFeO_3$ type oxides because of their important technological applications, recently received much attention. $LaGaO_3$ is used as a substrate material for the epitaxial growth of high temperature superconducting thin films [24], due to a small lattice mismatch. When doped with lower valence cations it exhibits high oxide ionic conductivity [25], as a good candidate material for use in solid oxide fuel cells (SOFCs) [26,27]. On the other hand, $LaInO_3$ is also considered as an electrolyte for SOFCs [28]. In addition, $LaInO_3$ is an excellent dielectric layer, along with $BaSnO_3$ as the semiconducting layer having similar in-plane lattice parameters, for an all-perovskite epitaxial field effect transistor [29].

In this study, we present a comprehensive study of structural, mechanical, electronic, optical, and lattice dynamical properties of $GdFeO_3$ type $LaMO_3$ (M=Ga and In) compounds whose bulk structures are stable in orthorhombic phase which conforms to *Pbnm* space group. The details of the calculations and some numerical parameters which are used in the calculations are given in the second section. Then the examined structural, mechanical, electronic, optical, and dynamical properties are discussed in the third section. Finally, a summary of the results is presented in the conclusions section.

2. Computational details

The basis of the calculations in this work are based on density functional theory (DFT) in which Kohn-Sham equations are solved numerically and iteratively [30,31]. The solution has been obtained by calculating the total energy as implemented in VASP (Vienna Ab initio Simulation Package) [32,33] software using plane-wave basis set and psuedopotential approach. For all the calculations presented in this study, we use Perdew, Burke and Ernzerhof [34] type pseudopotentials for all atoms in the framework of Generalized Gradient Approximation (GGA) of the exchange-correlation potential.

After the optimization of our complex compounds in five different phases, energy-volume data is fitted to Vinet equation of state. After determining the stable phase, phase transition pressures have also been calculated from enthalpy–pressure graphs. Then, their

full structural, mechanical, electronic, optical, and vabrational properties have been studied in stable orthorhombic phase which conforms to *Pbnm* space group. In these calculations, Brillouin zone integration have been performed with automatically generated 10 × 10 × 10 *k*-point mesh for cubic; 10 × 10 × 8 *k*-point mesh for tetragonal and hexagonal phases, and 8 × 6 × 8 *k-po*int mesh for rhombohedral and orthorhombic phases, respectively, all centered at Γ-point following the convention of Monkhorst and Pack [35]. 800 eV is taken for the electron kinetic energy cut-off value for expansion of the electron wave functions. Methfessel–Paxton type smearing is applied on fermionic occupation function with 0.27 eV smearing parameter. The crystal structures of these complex alloys in cubic (*Pm-3m*), tetragonal (*P4mm*), hexagonal (*P-3m1*) phases with 5-atom primitive cell, rhombohedral (*R-3c*) phase with 10-atom primitive cell, and orthorhombic (*Pbnm*) phase with 20-atom primitive cell are presented in Figure 1(a)–(e), respectively.

GGA or LDA functionals often fail to describe the strongly correlated electron systems with localized d orbitals accurately. In such a case, the on-site Coulomb interaction with an effective Hubbard *U* parameter (GGA + *U* or L(S)DA + *U*) is included using the approach of Dudarev et al. [36] in which the on-site Coulomb (*U*) and exchange (*J*) parameters are not taken into account separately, since only the difference (*U* – *J*) is physically meaningful. Therefore, we have taken into account a single parameter $U_{eff} = (U - J)$. In examining our compounds, we use U_{eff} = 6 eV for d-orbitals of La atoms.

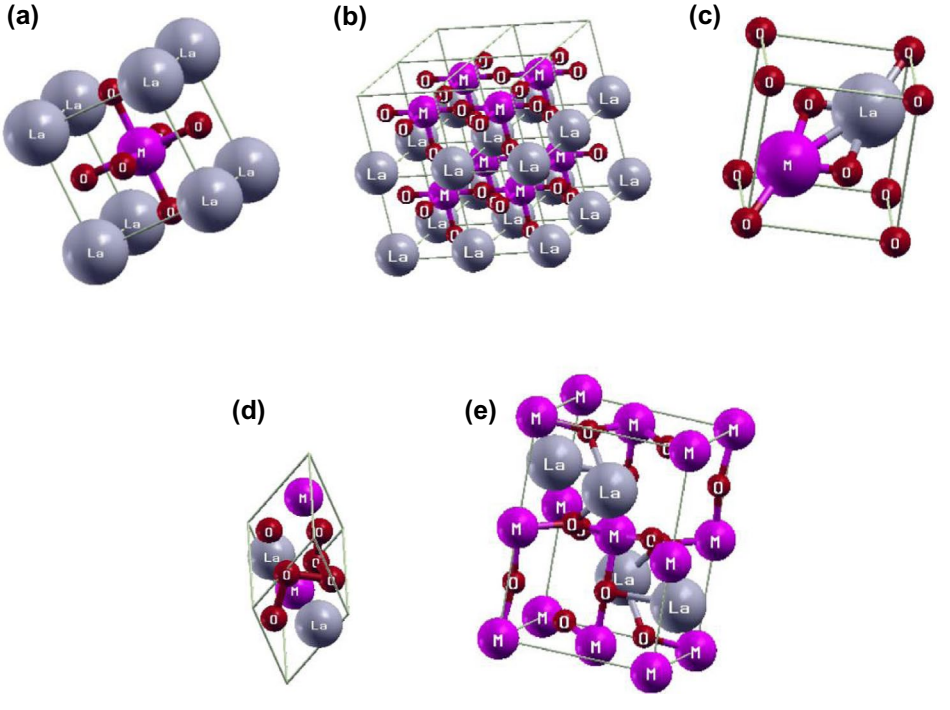

Figure 1. (colour online) The crystal structure of $LaMO_3$ in; (a) cubic *Pm-3m* space group, (b) tetragonal *P4mm* space group, (c) hexagonal *P-3m1* space group, (d) rhombohedral *R-3c* space group, (e) orthorhombic *Pbnm* space group.

Table 1. The calculated cohesive and formation energies of $LaGaO_3$ and $LaInO_3$ systems.

Material	Crystal structure	E_{coh} (eV/formula unit)	E_{for} (eV/formula unit)
$LaGaO_3$	Cubic (*Pm-3m*)	−31.08	−13.55
	Tetragonal (*P4mm*)	−31.08	−13.55
	Hexagonal (*P-3m1*)	−30.49	−12.97
	Rhombohedral (*R-3c*)	−31.33	−13.81
	Orthorhombic (*Pbnm*)	−31.35	−13.83
$LaInO_3$	Cubic (*Pm-3m*)	−28.19	−11.00
	Tetragonal (*P4mm*)	−29.04	−11.84
	Hexagonal (*P-3m1*)	−29.55	−12.36
	Rhombohedral (*R-3c*)	−29.54	−12.35
	Orthorhombic (*Pbnm*)	−29.79	−12.60

3. Results and discussion

Goldschmidt tolerance factor [37] is defined for a rough prediction of the formation of perovskite type alloys and is given by

$$t = \frac{(r_A + r_B)}{\sqrt{2}(r_B + r_O)} \tag{1}$$

where r_A, r_B and r_O are the ionic radii of the A, B cations, and oxygen anion, respectively. If this value is between 0.9 and 1.0, the examining structure is energetically favored in cubic phase [38,39] and if this value is between 0.71 and 0.9, the structure is expected to be energetically favored in orthorhombic phase [38]. The calculated Goldschmidt tolerance factors for $LaGaO_3$ and $LaInO_3$ systems are 0.85 and 0.78, respectively. This implies that these compounds can be crystallized in orthorhombic phase very likely.

The stability of a crystal can be determined from cohesive energy and it is known that if the absolute value of the cohesive energy of a structure is larger than that of others it can be said to be more stable [40,41]. Also, the formation energy can be used to determine the crystal stability [42] in a similar fashion. The cohesive and formation energies of a solid compound whose chemical formula is A_xB_y, are given by the following formulas, respectively,

$$E_{\text{coh}} = E_{\text{tot}} - \left(xE_{\text{A}} + yE_{\text{B}}\right) \tag{2}$$

and

$$E_{\text{for}} = E_{\text{tot}} - \left(xE_{\text{A}}^{\text{bulk}} + yE_{\text{B}}^{\text{bulk}}\right) \tag{3}$$

where, E_{tot} is the total energy of the unit cell. E_{A} and E_{B} are the energies of the isolated A and B atoms, respectively. $E_{\text{A}}^{\text{bulk}}$and $E_{\text{B}}^{\text{bulk}}$ are the energies of A and B atoms in the ground state crystal structure. Therefore, we have calculated cohesive and formation energies of our compounds in five different phases to determine the most stable structure. These energies are given in Table 1. It is clearly seen that E_{for} and E_{coh} energies of these compounds in orthorhombic phase are smaller than the energy values of other phases. In this regard, further properties of our materials have been examined in the stable orthorhombic (*Pbnm*) phase.

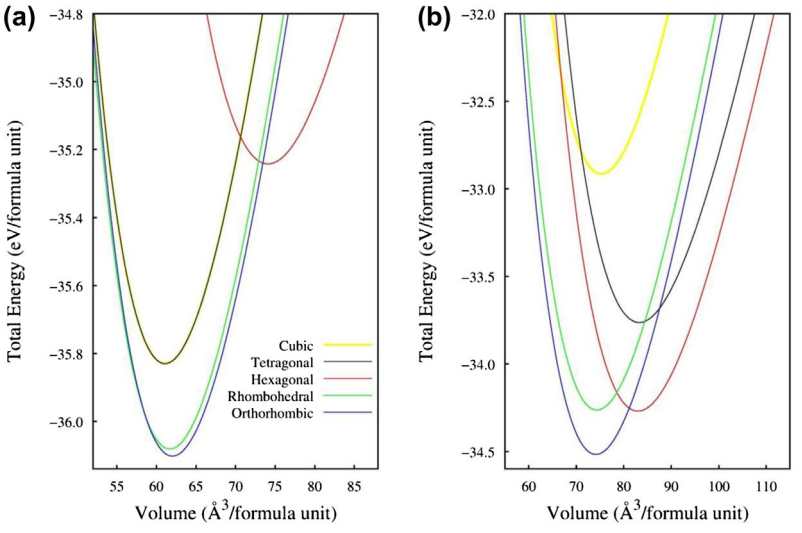

Figure 2. (colour online) Total energies as a function of volume for various possible structures of (a) $LaGaO_3$ and (b) $LaInO_3$.

Table 2. The structural parameters of $LaGaO_3$ and $LaInO_3$ in cubic (*Pm-3m*) phase.

Material	Reference	*a* (Å)	*B* (GPa)	*B*′
$LaGaO_3$	This work	3.937	189.236	4.626
	Experimental [46,47]	3.874	–	–
	Theoretical [46,47]	3.915	–	–
	Theoretical [48]	3.866	–	–
	Theoretical [49]	3.874	194.40	
$LaInO_3$	This work	4.221	154.202	4.620
	Experimental [46,47]	4.110	–	–
	Theoretical [46]	4.105	–	–
	Theoretical [49]	4.110	158.00	

Table 3. The structural parameters of $LaGaO_3$ and $LaInO_3$ in tetragonal (*P4mm*) phase.

Material	Reference	*a* (Å)	*c* (Å)	*B* (GPa)	*B*′
$LaGaO_3$	This work	3.937	3.937	189.237	4.626
$LaInO_3$	This work	3.951	5.328	130.417	4.563

Table 4. The structural parameters of $LaGaO_3$ and $LaInO_3$ in hexagonal (*P-3m1*) phase.

Material	Reference	*a* (Å)	*c* (Å)	*B* (GPa)	*B*′
$LaGaO_3$	This work	3.625	6.246	143.419	4.635
$LaInO_3$	This work	3.701	6.690	131.479	4.630

Table 5. The structural parameters of $LaGaO_3$ and $LaInO_3$ in rhombohedral (*R-3c*) phase.

Material	Reference	*a* (Å)	$\alpha = \beta = \gamma$	*B* (GPa)	*B*′
$LaGaO_3$	This work	5.548	60.9°	183.112	4.597
$LaInO_3$	This work	5.883	61.4°	151.934	4.599

Table 6. The structural parameters of $LaGaO_3$ and $LaInO_3$ in orthorhombic (*Pbnm*) phase.

Material	Reference	*a* (Å)	*b* (Å)	*c* (Å)	*B* (GPa)	*B′*
$LaGaO_3$	This work	5.594	7.909	5.603	181.723	4.601
	Experimental [50]	5.473	7.767	5.526	–	–
	Theoretical [50]	5.465	7.737	5.561	–	–
	Theoretical [51]	5.507	7.806	5.529	–	–
$LaInO_3$	This work	5.814	8.394	6.069	153.006	4.625
	Experimental [50]	5.723	8.207	5.914	–	–
	Theoretical [50]	5.700	8.182	5.939	–	–
	Theoretical [51]	5.804	8.227	5.828	–	–

3.1. Structural and mechanical properties

After the optimization processes of $LaMO_3$ (M=Ga and In) compounds in different five phases with GGA + *U* method (U_{eff} = 6 eV), the stable phase is determined by plotting energy–volume graphs as seen in Figure 2. In DFT calculations, the Hubbard-U parameter for any atom is chosen approximately, so this parameter has not an exact value generally and is subject to change according to the system of interest. In our case, the strength of the intra-site repulsion (U_{eff}) for La-d orbitals is determined by considering previous studies on similar structures. The lattice parameters and some structural constants are calculated by fitting Vinet equation of state [43–45] which is given by Equations (4) and (5). The calculated parameters of different phases are presented in Tables 2–6.

$$E(V) = E_0 + \frac{9BV_0}{\xi^2}\left[1 + \{\xi(1-x) - 1\}\exp\{\xi(1-x)\}\right] \tag{4}$$

$$P(V) = \left\{\frac{3B(1-x)}{x^2}\right\}\exp\{\xi(1-x)\} \tag{5}$$

where E_0 and V_0 are the zero pressure equilibrium energy and volume, respectively, $x = \left(\frac{V}{V_0}\right)^{1/3}$ and $\xi = \frac{3}{2}\left(B' - 1\right)$, *B* is the bulk modulus and *B′* is its pressure derivative.

The energetic behavior of cubic and tetragonal phases is very similar and the hexagonal phase seems to be unstable with rather large ground state energy. The orthorhombic phase is the most stable phase for $LaGaO_3$ compound with slightly lower energy than rhombohedral structure as seen in Figure 2(a). The cubic phase is unstable for $LaInO_3$, while the orthorhombic phase is the stable one for this compound also, as seen in Figure 2(b). E_{for} and E_{coh} energies of these compounds show the same behavior, as seen in Table 1. E_{for} and E_{coh} energies and also the fitted curves show that the orthorhombic phase (*Pbnm*) is the stable phase for both of these materials.

As a result of our calculations for cubic (*Pm-3m*) phase, the lattice parameters of $LaGaO_3$ and $LaInO_3$ are obtained with %1.6 and %2.7 differences from experimental results, respectively.

The lattice parameters (*a*, *b*, and *c*) of $LaGaO_3$ and $LaInO_3$ in stable orthorhombic (*Pbnm*) phase are also obtained with deviations from experimental results as %2.2, %1.8, %1.4 and %1.6, %2.2, %2.6, respectively. The relatively high bulk moduli of these compounds show that these materials are hard materials. Also, both of these materials have big pressure

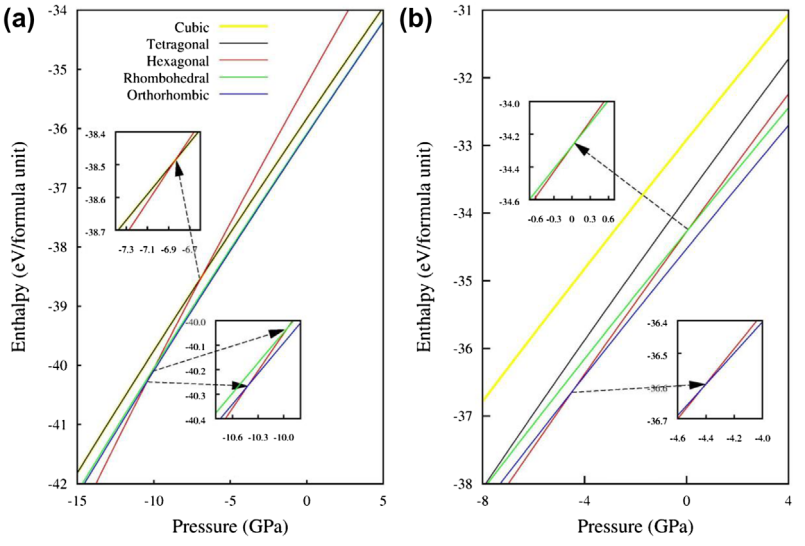

Figure 3. (colour online) Enthalpies as a function of pressure of various possible structures of (a) $LaGaO_3$ and (b) $LaInO_3$.

derivative of bulk modulus and it indicates that, they show strong sensitivity against pressure change. Then phase transition pressures have been calculated from enthalpy–pressure graphs as seen in Figure 3.

At zero pressure, the enthalpies of $LaGaO_3$ and $LaInO_3$ in the orthorhombic phase (*Pbnm*) as seen in Figure 3(a) and (b), respectively, are minimum as expected. In Figure 3(a), at a pressure of –6.88 GPa, the enthalpies of hexagonal, cubic, and tetragonal phases of $LaGaO_3$ compound become equal. Also, the enthalpies are equal at –10.43 GPa for hexagonal and orthorhombic phases and at –9.96 GPa for rhombohedral and hexagonal structures. In Figure 3(b), at –4.43 GPa, the enthalpies of $LaInO_3$ compound are equal for hexagonal and orthorhombic phases. Likewise, the enthalpies of hexagonal and rhombohedral phases are equal at 0.036 GPa. The negative pressure values correspond to extended lattices. But it is clearly seen that the orthorhombic phase remains stable in a wide range of positive pressures for both compounds.

The mechanical and dynamical behaviors of a crystal can be explained in terms of its elastic constants. They can give detailed information about the stability, hardness or stiffness of the materials. These constants can be obtained from *ab initio* calculations by using the 'stress–strain' method [52] with great accuracy and precision. The calculated second order elastic constants of orthorhombic $LaGaO_3$ and $LaInO_3$ are given in Table 7.

The mechanical stability of a crystal or durability against external forces is a desirable situation in technological applications. The mechanical stability conditions of a crystal structure depend on its elastic constants and also these conditions are different from each other for different structures. Since the crystal is stable mechanically, the Born's stability criteria [53] must be ensured. Mechanical stability criteria of a orthorhombic crystal are given by

$$c_{ii} < 0 \text{ and } \left(c_{ii} + c_{ij} - 2c_{ij} < 0\right) \quad \text{for } i = 1 \ldots 6 \tag{6}$$

Table 7. The calculated elastic constants of $LaGaO_3$ and $LaInO_3$ in stable orthorhombic (*Pbnm*) phase.

(GPa)	$LaGaO_3$	$LaInO_3$
C_{11}	301.18	225.81
C_{12}	136.27	104.38
C_{13}	116.24	121.69
C_{22}	263.95	195.28
C_{23}	104.43	111.46
C_{33}	242.27	238.12
C_{44}	72.20	58.90
C_{55}	94.67	70.37
C_{66}	91.43	52.61

Both of our materials have satisfied these criteria for mechanical stability. Also bulk (B) and shear modulus (G) of a solid crystal in the orthorhombic phase can be calculated with Voigt [54] -Reuss [55] -Hill [56] relations as given in Equations 7–10. The Voigt and Reuss approximations present upper and lower limits, respectively, for calculating B and G values of the crystal.

$$B_R = \frac{1}{(s_{11} + s_{22} + s_{33}) + 2(s_{12} + s_{13} + s_{23})} \tag{7}$$

$$B_V = \frac{1}{9}(c_{11} + c_{22} + c_{33}) + \frac{2}{9}(c_{12} + c_{13} + c_{23}) \tag{8}$$

$$G_R = \frac{15}{4(s_{11} + s_{22} + s_{33}) - 4(s_{12} + s_{13} + s_{23}) + 3(s_{44} + s_{55} + s_{66})} \tag{9}$$

$$G_V = \frac{1}{15}(c_{11} + c_{22} + c_{33} - c_{12} - c_{13} - c_{23}) + \frac{1}{5}(c_{44} + c_{55} + c_{66}) \tag{10}$$

In Equations 6–10, the c_{ij} values are the elastic constants, and the s_{ij} are the elastic compliance constants of a orthorhombic crystal in Equations 7 and 9. Using energy considerations, Hill [56] approximation is a practical method to estimate the bulk and shear moduli of a crystal, so the elastic moduli of the polycrystalline material can be approximated. Therefore, shear moduli can be calculated from $G = \frac{1}{2}(G_V + G_R)$ and bulk moduli from the expression $B = \frac{1}{2}(B_V + B_R)$.

Moreover, Young's modulus [57] E and Poisson's ratio [57] ν of an isotropic material can be calculated by using estimated bulk and shear moduli as seen in Equations 11 and 12, respectively.

$$E = \frac{9BG}{3B + G} \tag{11}$$

$$\nu = \frac{3B - 2G}{2(3B + G)} \tag{12}$$

Table 8. The calculated upper and lower limits, average values of bulk and shear moduli, Young's moduli and Poisson's ratios of $LaGaO_3$ and $LaInO_3$ in stable orthorhombic (*Pbnm*) phase.

	$LaGaO_3$	$LaInO_3$
B_V (GPa)	169.03	148.25
B_R (GPa)	166.07	146.25
B (GPa)	167.55	147.25
G_V (GPa)	81.69	57.82
G_R (GPa)	80.31	56.95
G (GPa)	81.00	57.38
E (GPa)	209.29	152.36
v	0.291	0.327

Table 9. The calculated shear anisotropic factors in different planes, longitudinal, transverse, and average wave velocities in crystal and also Debye temperatures for $LaGaO_3$ and $LaInO_3$ in stable orthorhombic (*Pbnm*) phase.

	$LaGaO_3$	$LaInO_3$
A_1 (1 0 0)	0.928	1.068
A_2 (0 1 0)	1.273	1.337
A_3 (0 0 1)	1.250	0.991
v_l (m/s)	5122.86	4257.38
v_t (m/s)	2777.54	2155.99
v_m (m/s)	3099.25	2416.78
Θ_D (K)	459.17	358.10

Estimated upper and lower limits and the average bulk and shear moduli with Hill approximation [56] along with the calculated Young's modulus (E) and Poisson's ratio (v) are given in Table 8.

Young's modulus is also known as the ratio of stress and strain, and is used to define the stiffness of the solid. The calculated Young's modulus values for $LaGaO_3$ and $LaInO_3$ are 209.29 and 152.36 GPa, respectively. Bulk, shear, and Young's moduli of our materials show that $LaGaO_3$ compound is stiffer than $LaInO_3$ compound in orthorhombic (*Pbnm*) phase. B/G ratio [58,59] and Pugh's ratio ($k = G/B$) [58–62] include very important information about stiffness of the materials. B/G ratio of $LaGaO_3$ and $LaInO_3$ are 2.06 and 2.56 and also Pugh's ratio ($k = G/B$) of these compounds are 0.48 and 0.39, respectively. These values indicate that $LaGaO_3$ and $LaInO_3$ are ductile materials in orthorhombic (*Pbnm*) phase.

Poisson's ratios [63,64] of $LaGaO_3$ and $LaInO_3$ are found to be 0.291 and 0.327, respectively. These values indicate that both materials have ionic character. Especially the ionic character is more dominant in $LaGaO_3$ compound, than that in $LaInO_3$.

Shear anisotropic factors [64], ultrasonic wave velocities [65,66], and Debye temperatures [66] of $LaGaO_3$ and $LaInO_3$ are calculated by using Equations 13–19 and given in Table 9. The shear anisotropic factors in different planes of crystals tell us the degree of elastic anisotropy of a material. Shear anisotropic factor (A_1) for the (1 0 0) plane is

$$A_1 = \frac{4c_{44}}{c_{11} + c_{33} - 2c_{13}} \tag{13}$$

Shear anisotropic factor (A_2) for the (0 1 0) plane is

$$A_2 = \frac{4c_{55}}{c_{22} + c_{33} - 2c_{23}} \tag{14}$$

and shear anisotropic factor (A_3) for the (0 0 1) plane is

$$A_3 = \frac{4c_{66}}{c_{11} + c_{22} - 2c_{12}} \tag{15}$$

A_1, A_2, A_3 values of our compounds indicate that especially for (1 0 0) plane, our materials have lower elastic anisotropy than (0 1 0) and (0 0 1) planes. However, both of our materials have anisotropic character mechanically.

The longitudinal and transverse wave velocities in a crystal are obtained from Navier's equation [65] as follows:

$$v_l = \left(\frac{B + \frac{4G}{3}}{\rho} \right)^{1/2} \tag{16}$$

and

$$v_t = \left(\frac{G}{\rho} \right)^{1/2} \tag{17}$$

and the average wave velocity [66] in the crystal is given by

$$v_m = \left[\frac{1}{3} \left(\frac{2}{v_t^3} + \frac{1}{v_l^3} \right) \right]^{-1/3} \tag{18}$$

where ρ is the density of the material. Finally, the Debye temperature is a fundamental parameter of a material and is estimated using the expression

$$\theta_D = \frac{h}{k} \left[\frac{3n}{4\pi} \left(\frac{N_A \rho}{M} \right) \right]^{1/3} v_m \tag{19}$$

where h is the Planck's constant, k is the Boltzmann's constant, N_A is the Avogadro's number, M is the molecular weight and n is the number of atoms in the molecule.

3.2. Electronic structure

In this section, the electronic band structures and total DOS of $LaGaO_3$ and $LaInO_3$ in the orthorhombic (*Pbnm*) structure are shown in Figure 4. The calculated spin-polarized electronic band structures of these materials are given along the high symmetry directions in the first Brillouin zone. Also electronic partial DOS of these systems are shown in Figure 5. The distribution of majority and minority spin channels are similar for our complex systems and this situation is mainly due to non magnetic characters of the systems. It is shown that there are energy gaps in both systems. They are found to be 3.14 and 2.55 eV for $LaGaO_3$ and $LaInO_3$, respectively. Therefore, these systems can be regarded as insulators. The electronic band gaps of both $LaGaO_3$ and $LaInO_3$ systems are indirect band gap from Γ to U point. O-p states are dominant below the Fermi level and also La-d states are dominant above the Fermi level for these $GdFeO_3$ type perovskite oxides, as seen in Figure 5.

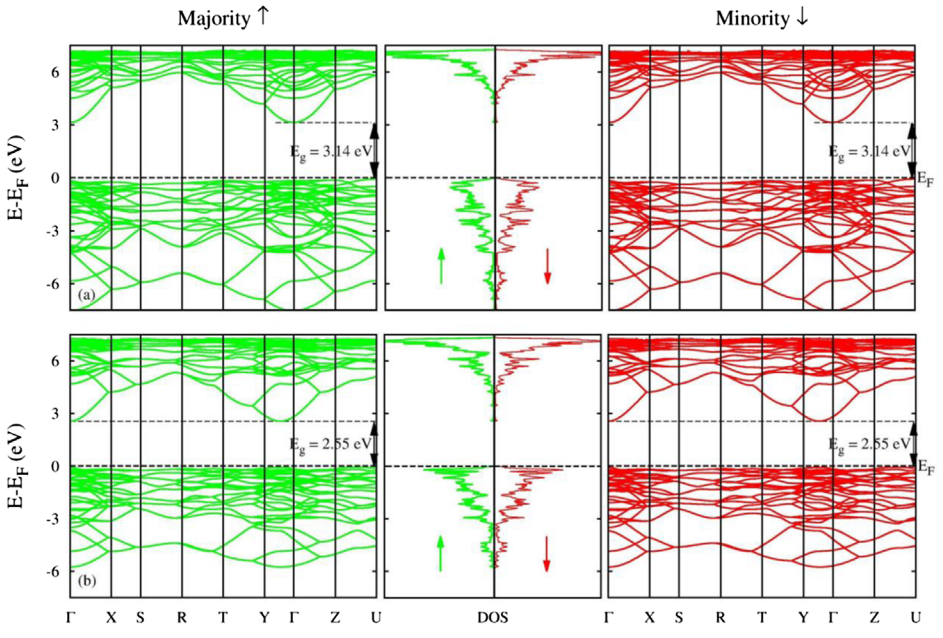

Figure 4. (colour online) The electronic band structures of (a) $LaGaO_3$ and (b) $LaInO_3$.

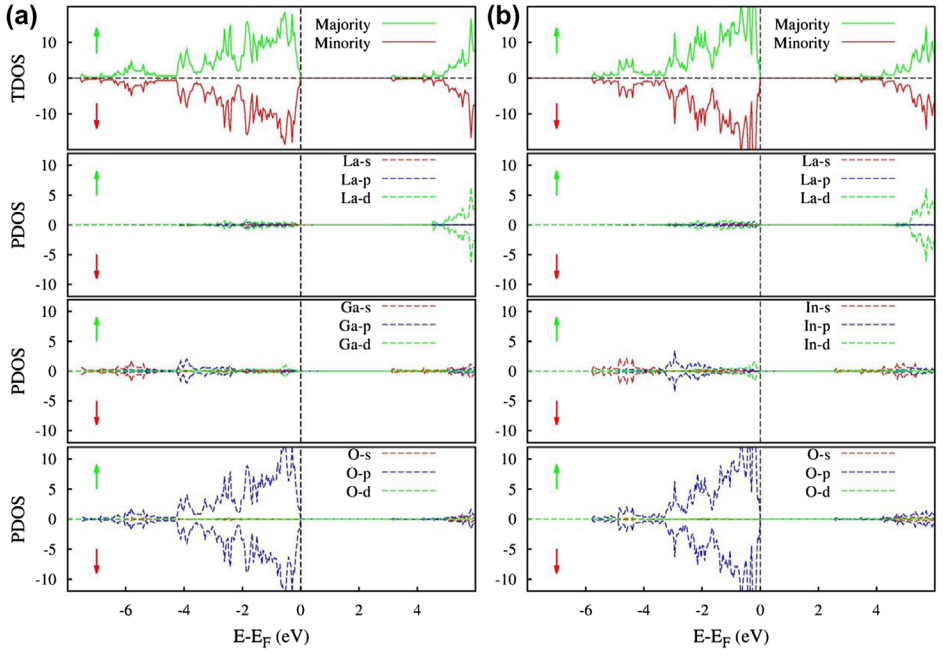

Figure 5. (colour online) Partial DOS of (a) $LaGaO_3$ and (b) $LaInO_3$.

In the valance band which is below Fermi level and in the conduction band which is above Fermi level, it is seen that Ga and In elements which belong to group-III elements don't have much effect on the electronic band configuration. Also there is a little hybridization

between O-p and La-d states just below and above Fermi level. Finally, there is Ga-p and In-p states at −4 and −3 eV energy levels, respectively.

3.3. Dielectric function and optical properties

It is well known that the frequency dependent dielectric function of a medium, which is given by Equation 20, can determine its optical response at all photon energies.

$$\varepsilon(\omega) = \varepsilon_r(\omega) + i\varepsilon_i(\omega) \tag{20}$$

There is a direct relationship between the electronic band structure and the imaginary part $\varepsilon_i(\omega)$ of the dielectric function of a material. Latter describes the optical absorptive behavior of a material and is given [67,68] by

$$\varepsilon_i(\omega) = \left(\frac{4\pi^2 e^2}{m^2\omega^2}\right) \sum_{i,j} \int_k i|M|j^2 f_i\left(1 - f_i\right)\delta\left(E_{j,k} - E_{i,k} - \omega\right)\mathrm{d}^3\mathbf{k} \tag{21}$$

where M is the dipole matrix, i and j are the initial and final states, respectively, fi is the Fermi distribution function for the ith state, E_i is the energy of the electron in the ith state and $\mathbf{k}$ is the crystal wave vector.

The real part $\varepsilon_r(\omega)$ of the dielectric function can be calculated using the Kramers-Kronig transformation [69,70].

$$\varepsilon_r(\omega) = 1 + \frac{2}{\pi} P \int_0^\infty \frac{\omega' \varepsilon_i(\omega')}{\omega'^2 - \omega^2} \mathrm{d}\omega' \tag{22}$$

where P denotes the principle value of the integral. The calculated frequency dependent optical properties give helpful information about the internal structure of the compounds.

The calculated frequency dependent dielectric function without local effects along x, y, z crystal axes as functions of photon energy in the 0–50 eV range are shown in Figure 6(a) and (b) for $LaGaO_3$ and $LaInO_3$, respectively. The imaginary part $\varepsilon_i(\omega)$ gives the information of absorptive behavior of $LaGaO_3$ and $LaInO_3$ systems. The threshold energies for the imaginary part of the dielectric function occur at 3.14 and 2.55 eV for $LaGaO_3$ and $LaInO_3$, respectively, which are consistent with the band gap values obtained from electronic band structure calculations. It is well known that, if a material system has a band gap larger than 3.1 eV, it works well in applications in the ultraviolet (UV) region of the spectrum [71,72]. In this respect, $LaGaO_3$ compound seems to be a suitable material for the high frequency UV device applications because of its wide band gap. There are strong absorption peaks located at 7.0 and 6.4 eV for $LaGaO_3$ and $LaInO_3$, respectively. There also appear small peaks around 20 eV energy level. Both of our compounds can be used for filtering applications for various energies in the UV spectrum.

The calculated real part of the frequency dependent dielectric function $\varepsilon_r(\omega)$ of $LaGaO_3$ and $LaInO_3$ compounds are given in Figure 6(a) and (b), respectively. It provides information about electronic polarizibility of a material. At zero frequency ($\omega = 0$), the static dielectric constants of $LaGaO_3$ and $LaInO_3$ compounds are obtained as $\varepsilon_r(0) = 5$ and $\varepsilon_r(0) = 4.8$, respectively. From these limit values, the real part of the dielectric function of $LaGaO_3$ and $LaInO_3$ compounds begin to increase and reach the maximum values at energies of 5.8 and

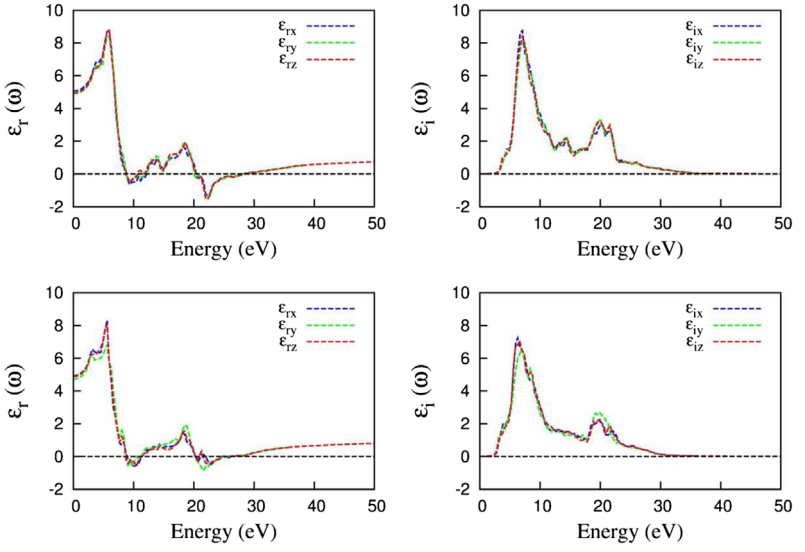

Figure 6. (colour online) The real and imaginary parts of the frequency dependent dielectric function of (a) $LaGaO_3$ and (b) $LaInO_3$.

5.5 eV, respectively. Then, the real part of the dielectric function of $LaGaO_3$ starts decreasing to zero and it takes negative values between 8.9 and 12 eV, and also between 20.2 and 28 eV. Similarly, the real part of the dielectric function of $LaInO_3$ starts decreasing to zero and it takes negative values between 8.7 and 11.5 eV, and also between 20.2 and 24.9 eV.

Then we calculated other optical properties of $LaGaO_3$ and $LaInO_3$ compounds by using Equations 23–27 which are plotted in Figure 7(a) and (b), respectively. These are reflectivity [73] $R(\omega)$, the absorption coefficient [73] $\alpha(\omega)$, the refractive index [73] $n(\omega)$, the extinction coefficient [73] $k(\omega)$ and the energy loss function [74] $L(\omega)$ which are given by:

$$R(\omega) = \left| \frac{\sqrt{\varepsilon(\omega)} - 1}{\sqrt{\varepsilon(\omega)} + 1} \right|^2, \tag{23}$$

$$\alpha(\omega) = \omega \sqrt{2 \sqrt{\varepsilon_r^2(\omega) + \varepsilon_i^2(\omega)} - 2\varepsilon_r(\omega)}, \tag{24}$$

$$n(\omega) = \sqrt{\frac{\sqrt{\varepsilon_r^2(\omega) + \varepsilon_i^2(\omega)} + \varepsilon_r(\omega)}{2}}, \tag{25}$$

$$k(\omega) = \sqrt{\frac{\sqrt{\varepsilon_r^2(\omega) + \varepsilon_i^2(\omega)} - \varepsilon_r(\omega)}{2}}, \tag{26}$$

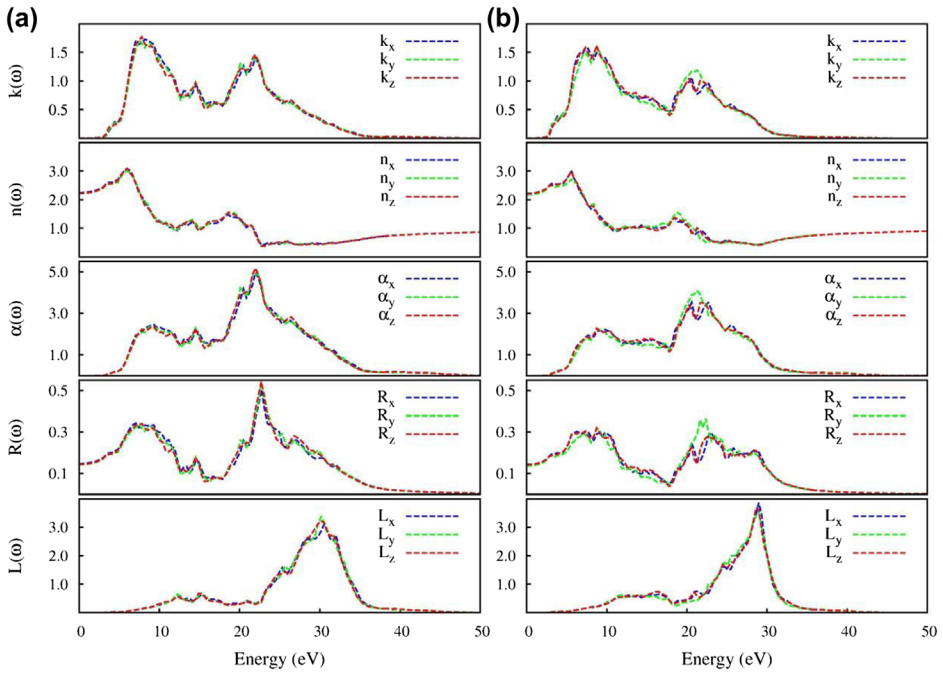

Figure 7. (colour online) The calculated optical parameters as a function of the frequency of (a) $LaGaO_3$ and (b) $LaInO_3$. Here, $R(\omega)$ is the reflectivity coefficient, $a(\omega)$ is the absorption coefficient and is given in m^{-1} divided by 10^7, $n(\omega)$ is the refractive index, $k(\omega)$ is the extinction coefficientand $L(\omega)$ the energy loss function.

$$L(\omega) = \frac{\varepsilon_i(\omega)}{\varepsilon_r^2(\omega) + \varepsilon_i^2(\omega)}. \tag{27}$$

We observed that, $LaGaO_3$ compound is optically isotropic although it is anisotropic mechanically. So, this material can be a good candidate for scintillator applications [75]. However, it can be said that $LaInO_3$ compound is optically anisotropic, since all of its optical properties in *y* direction are different from those in x and *z* directions. The refractive index $n(\omega)$ values of both $LaGaO_3$ and $LaInO_3$ compounds are almost constant in the lower energy region, then start increasing and after reaching maximum values in the UV region at about 6 and 5.5 eV, respectively, they decrease in the higher energy region. The static refractive indices $n(0)$ obtained for $LaGaO_3$ and $LaInO_3$ compounds are the same and are equal to 2.2. Generally, the refractive index of any material increases with the electron density. In addition, it is also related to chemical bonding properties. In general, ionic compounds have lower refractive index $n(\omega)$ values than covalent bonded compounds. To this end, both compounds have ionic character as already deduced before in Section 3.1 by considering their Poission's ratios. Finally, the $LaGaO_3$ compound can be considered transparent, since its refractive index $n(\omega)$ is independent of crystal directions.

The imaginary part of the dielectric function $\varepsilon_i(\omega)$ and the extinction coefficient $k(\omega)$ of these compounds have similar trends. The maximum values of the extinction coefficient $k(\omega)$ of $LaGaO_3$ and $LaInO_3$ compounds are located at 8.2 and 8.6 eV, respectively.

The zero-frequency optical reflectivities $R(0)$of $LaGaO_3$ and $LaInO_3$ compounds are 15 and 14%, respectively, and they remain nearly constant up to 2 eV. Then, they start to

increase reaching maximum values of 54% at 22.5 eV and 36% at 22 eV, respectively, whereas the real part of the dielectric function for both compounds are negative.

The energy loss function $L(\omega)$ gives an important information about the energy loss of a fast electron traversing in a material. The maximum peak in the energy loss $L(\omega)$ spectra can be associated with the plasmon peak [76]. The plasma resonances for the $LaGaO_3$ and $LaInO_3$ compounds occur at 30 and 29 eV, respectively.

Finally in this section, the absorption spectra of the $LaGaO_3$ and $LaInO_3$ compounds are plotted, which give information about scintillating characteristics of the material of interest. The maximum absorptions of $LaGaO_3$ and $LaInO_3$ compounds occur at 22 and 21.5 eV, respectively. These spectra show that, the $LaGaO_3$ compound is isotropic, while the $LaInO_3$ compound is an anisotropic material since the maximum absorption peak at 21.5 eV is along y-direction and it is larger than those of along x- and z-directions.

3.4. The lattice dynamical properties

The structural stability of a single crystalline material can be examined by evaluating the lattice dynamical properties. In this respect, we calculated the phonon dispersion spectra of $LaGaO_3$ and $LaInO_3$ compounds in stable orthorhombic (*Pbnm*) phase. The presented phonon frequencies are estimated using PHONOPY program [77] based on the interatomic force constants. The force constants and vibrational frequencies are obtained within the linear response method of the density functional perturbation theory [77–80]. A $2 \times 1 \times 2$ super-cell is used to calculate full phonon spectra along the main symmetry directions in irreducible Brillouin zone. The phonon dispersion curves and atom projected vibrational DOS are given in Figure 8(a) and (b) for $LaGaO_3$ and $LaInO_3$ compounds, respectively. To the best of our knowledge, there is not any study in the literature investigating the phonon

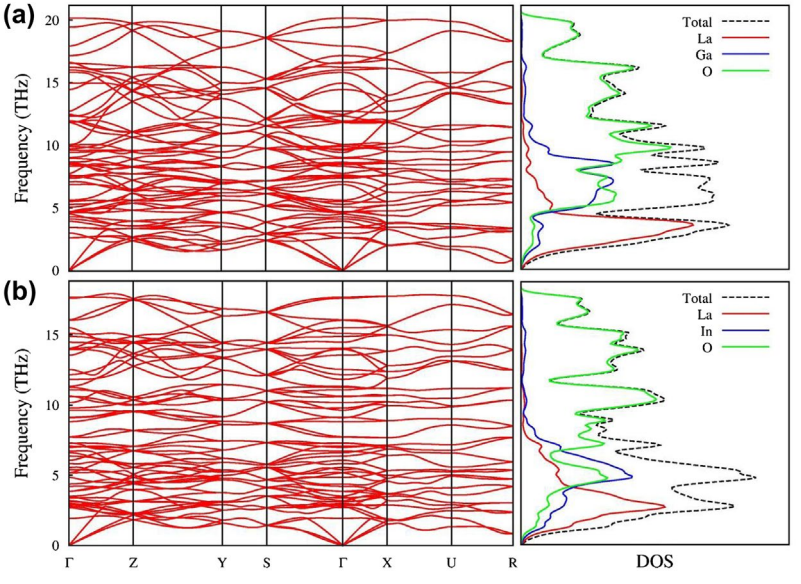

Figure 8. (colour online) Phonon dispersion curves along high symmetry directions in the first Brillion zone of (a) $LaGaO_3$ and (b) $LaInO_3$.

properties of these compounds, so we are not able to make any comparison due to lack of data on dynamics of these systems.

It is seen from Figure 8(a) and (b) that $LaGaO_3$ and $LaInO_3$, respectively, have very similar phonon spectra and the phonon DOS. The calculated phonon dispersion curves do not show any vibrational anomaly or softening behaviour, confirming the dynamical stability of $LaGaO_3$ and $LaInO_3$ compounds in orthorhombic (*Pbnm*) phase. The primitive cell of $LaMO_3$ (M=Ga and In) is composed of 20 atoms yielding totally 60 phonon branches with 3 acoustic and 57 optical branches. No clear gap has been observed between optic and acoustic branches. The optical vibrations of La are largely located at the low energy regions around 2–4 THz due to high atomic mass of La atom compared to other atoms in composition. The energies of these optical modes of La are comparable to acoustic branches. The optical vibrations of oxygen spread over a wide energy range between 5 and 20 THz resulting from the low atomic mass of oxygen.

4. Conclusion

The structural, mechanical, electronic, optical, and lattice dynamical properties of the $GdFeO_3$ type $LaMO_3$ (M=Ga and In) lanthanum perovskite oxides in orthorhombic (*Pbnm*) phase have been investigated in detail. Firstly, these compounds have been studied in five different phases which are cubic (*Pm-3m*), tetragonal (*P4mm*), hekzagonal (*P-3m1*), rhombohedral (*R-3c*), and orthorhombic (*Pbnm*) phases. The ground states of both systems are predicted to be orthorhombic (*Pbnm*) phase considering the energy and enthalpy values. The calculated spin-polarized electronic band structures with (U_{eff} = 6 eV) show that both of our materials are non-magnetic insulators with 3.14 and 2.55 eV energy band gaps for $LaGaO_3$ and $LaInO_3$, respectively. The mechanical and optical properties of $LaGaO_3$ compound show that this compound has mechanically anisotropic character although it is optically isotropic. So this compound can be considered to be utilized in scintillator applications. On the other hand, $LaInO_3$ structure seems to be both mechanically and optically anisotropic material. The systems are also dynamically stable considering *ab initio* phonon dispersion curves in orthorhombic phase.

Disclosure statement

No potential conflict of interest was reported by the authors.

Funding

This work was supported by the Ahi Evran University Research Project Unit [project number PYO-KMY.4001.15.001].

References

[1] P.M. Woodward, *Octahedral tilting in perovskites. 1. Geometrical considerations*, Acta Cryst. B 53 (1997), pp. 32–43.
[2] M. Marezio, J.P. Remeika, and P.D. Dernier, *The crystal chemistry of the rare earth orthoferrites*, Acta Cryst. B 26 (1970), pp. 2008–2022.
[3] M. Itoh and Y. Hinatsu, *Crystal structures and magnetic properties of Ba1-ySryPrO3 (0 ≤ y ≤ 1.0)*, J. Alloys Compd. 264 (1998), pp. 119–124.

[4] T. Wolfram and Ş. Ellialtioglu, *Electronic and Optical Properties of D -Band Perovskites*, Cambridge, 2006.
[5] K.A. Müller, Th. von Waldkirch, W. Berlinger, and B.W. Faughnan, *Photochromic Fe5+(3d3) in SrTiO3 evidence from paramagnetic resonance*, Solid State Commun. 9 (1971), pp. 1097–1101.
[6] S. Kamimura, H. Yamada, and X. Chao-Nan, *Purple photochromism in Sr2SnO4:Eu3+ with layered perovskite-related structure*, Appl. Phys. Lett. 102 (2013), pp. 031110–031114.
[7] C.G. Granqvist, *Electrochromic tungsten oxide films: Review of progress 1993–1998*, Sol. Energy Mater. Sol. Cells 60 (2000), pp. 201–262.
[8] M.C. Rao, *Structure and properties of WO3 thin films for electrochromic device application*, J. Non-Oxide Glasses 5 (2013), pp. 1–8.
[9] V. Busico, C. Carfagna, V. Salerno, M. Vacatello, and F. Fittipaldi, *The layer perovskites as thermal energy storage systems*, Solar Energy 24 (1980), pp. 575–579.
[10] C. Liu, F. Li, M. Lai-Peng, and C. Hui-Ming, *Advanced materials for energy storage*, Adv. Mater. 22 (2010), pp. E28–E62.
[11] C.D. Chandler, C. Roger, and M.J. Hampden-Smith, *Chemical aspects of solution routes to perovskite-phase mixed-metal oxides from metal-organic precursors*, Chem. Rev. 93 (1993), pp. 1205–1241.
[12] N.A. Hill, Why are there so few magnetic ferroelectrics?, J. Phys. Chem. B 104 (2000), pp. 6694–6709.
[13] M. Dawber, K.M. Rabe, and J.F. Scott, *Physics of thin-film ferroelectric oxides*, Rev. Mod. Phys. 77 (2005), pp. 1083–1130.
[14] D. Damjanovic, *Ferroelectric, dielectric and piezoelectric properties of ferroelectric thin films and ceramics*, Rep. Prog. Phys. 61 (1998), pp. 1267–1324.
[15] A.J. Millis, *Lattice effects in magnetoresistive manganese perovskites*, Nature 392 (1998), pp. 147–150.
[16] S. Sato, R. Takahashi, M. Kobune, and H. Gotoh, *Basic properties of rare earth oxides*, Appl. Catal. A-Gen. 356 (2009), pp. 57–63.
[17] Y-F.Y. Yao, The oxidation of hydrocarbons and CO over metal oxides: IV. Perovskite-type oxides. J. Catal. 36 (1975), pp. 266–275, .
[18] G.N. Pirogova, R.I. Korosteleva, N.M. Panich, T.A. Lagutina, Y.V. Voronin, Catalytic oxidation of CO, hydrocarbons, and ethyl acetate over perovskite-type complex oxides. Russ. Chem. Bull. 43 (1994), pp. 551–554, .
[19] T. Harada, Y. Teraoka, and S. Kagawa, *Perovskite-type oxides as catalysts for selective reduction of nitric oxide by ethylene*, Appl. Surf. Sci. 121–122 (1997), pp. 505–508.
[20] K.K. Hansen, *Electrochemical reduction of nitrous oxide on La1-xSrxFeO3 perovskites*, Mater. Res. Bull. 45 (2010), pp. 1334–1337.
[21] J.G. Mavroides, J.A. Kafalas, and D.F. Kolesar, *Photoelectrolysis of water in cells with SrTiO3 anodes*, Appl. Phys. Lett. 28 (1976), pp. 241–243.
[22] J. Shi and L. Guo, *ABO3-based photocatalysts for water splitting*, Prog. Nat. Sci. 22 (2012), pp. 592–615.
[23] B. Yıldız, D.J. Myers, J.D. Carter, K.C. Chang, and H. You, *In situ X-ray and electrochemical studies of solid oxide fuel cell/electrolyzer oxygen electrodes*, Adv. Solid Oxise Fuel Cells III: Ceram. Eng. Sci. Proc. 28 (2008), pp. 153–164.
[24] M. Nieminen, S. Lehto, and L. Niinistö, *Atomic layer epitaxy growth of $LaGaO_3$ thin films*, J. Mater. Chem. 11 (2001), pp. 3148–3153; and the references therein.
[25] T. Ishihara, H. Matsuda, and Y. Takita, Doped LaGaO3 perovskite type oxide as a new oxide ionic conductor, J. Am. Chem. Soc. 116 (1994), pp. 3801–3803.
[26] H. Boysen, M. Lerch, R. Gilles, B. Krimmer, and D.M. Többens, *Structure and ionic conductivity in doped LaGaO3*, Appl. Phys. A 74 (2002), pp. S966–S968.
[27] H. He, X. Huang, and L. Chen, *Sr-doped LaInO3 and its possible application in a single layer SOFC*, Solid State Ionics 130 (2000), pp. 183–193.
[28] D. Lybye, F.W. Poulsen, and M. Mogensen, *Conductivity of A- and B-site doped LaAlO3, LaGaO3, LaScO3 and LaInO3 perovskites*, Solid State Ionics 128 (2000), pp. 91–103.
[29] U. Kim, C. Park, T. Ha, Y.m. Kim, N. Kim, C. Ju, J. Park, J. Yu, J.H. Kim, and K. Char, *All-perovskite transparent high mobility field effect using epitaxial $BaSnO_3$ and $LaInO_3$*, APL Mater. 3 (2015), pp. 036101-(1–7).

[30] W. Kohn and L.J. Sham, *Self-consistent equations including exchange and correlation effects*, Phys. Rev. 140 (1965), pp. A1133–A1138.
[31] P. Hohenberg and W. Kohn, *Inhomogeneous electron gas*, Phys. Rev. 136 (1964), pp. B864–B871.
[32] G. Kresse and J. Hafner, *Ab initio molecular dynamics for liquid metals*, Phys. Rev. B 47 (1994), pp. 558–561.
[33] G. Kresse and J. Furthmüller, *Efficiency of ab initio total energy calculations for metals and semiconductors using a plane-wave basis set*, Comp. Mater. Sci. 6 (1996), pp. 15–50.
[34] J.P. Perdew, K. Burke, and M. Ernzerhof, *Generalized gradient approximation made simple*, Phys. Rev. Lett. 77 (1996), pp. 3865–3868.
[35] H.J. Monkhorst and J.D. Pack, *Special points for Brillouin-zone integrations*, Phys. Rev. B 13 (1976), pp. 5188–5192.
[36] S.L. Dudarev, G.A. Botton, S.Y. Savrasov, C.J. Humphreys, and A.P. Sutton, *Electron-energy-loss spectra and the structural stability of nickel oxide: An LSDA+U study*, Phys. Rev. B 57 (1998), pp. 1505–1509.
[37] V.M. Goldschmidt, *Die Gesetze der Krystallochemie* [The laws of crystal chemistry], Die Naturwissenschaften 14 (1926), pp. 477–485.
[38] H. Kronmüller and S. Parkin (eds.), *Handbook of Magnetism and Advanced Magnetic Materials Vol. 4 Novel Materials*, John Wiley and Sons Ltd, Chichester, 2007.
[39] R.H. Buttner and E.N. Maslen, *Structural parameters and electron difference density in BaTiO3*, Acta Crystallogr. B 48 (1992), pp. 764–769.
[40] J. Feng, B. Xiao, J.C. Chen, and C.T. Zhou, *Theoretical study on the stability and electronic property of Ag2SnO3*, Solid State Sci. 11 (2009), pp. 259–264.
[41] S.F. Matar, R. Weihrich, D. Kurowski, and A. Pfitzner, *DFT calculations on the electronic structure of CuTe2 and Cu7Te4*, Solid State Sci. 6 (2004), pp. 15–20.
[42] E. Zhao and Z. Wu, *Electronic and mechanical properties of 5d transition metal mononitrides via first-principles*, J. Solid State Chem. 181 (2008), pp. 2814–2827.
[43] R.E. Cohen, O. Gülseren, and R.J. Hemley, *Accuracy of equation-of-state formulations*, Am. Mineral. 85 (2000), pp. 338–344.
[44] P. Vinet, J.H. Rose, J. Ferrante, and J.R. Smith, Universal features of the equation of state of solids, J. Phys. Condens. Matter 1 (1989), pp. 1941–1963.
[45] P. Vinet, J. Ferrante, J.H. Rose, and J.R. Smith, *Compressibility of solids*, J. Geophys. Res. 92 (1987), pp. 9319–9325.
[46] A.S. Verma and V.K. Jindal, *Lattice constant of cubic perovskites*, J. Alloys Compd. 485 (2009), pp. 514–518.
[47] R.L. Moreira and A. Dias, *Comment on "Prediction of lattice constant in cubic perovskites"*. J. Phys. Chem. Solids 68 (2007), pp. 1617–1622.
[48] L.Q. Jiang, J.K. Guo, H.B. Liu, M. Zhu, X. Zhou, P. Wu, and C.H. Li, *Prediction of lattice constant in cubic perovskites*, J. Phys. Chem. Solids 67 (2006), pp. 1531–1536.
[49] A.S. Verma and A. Kumar, *Bulk modulus of cubic perovskites*, J. Alloys Compd. 541 (2012), pp. 210–214.
[50] R. Ubic and G. Subodh, *The prediction of lattice constants in orthorhombic perovskites*, J. Alloys Compd. 488 (2009), pp. 374–379.
[51] A. Kumar and A.S. Verma, *Lattice constant of orthorhomic perovskite solids*, J. Alloys Compd. 480 (2009), pp. 650–657.
[52] Y.L. Page and P. Saxe, *Symmetry-general least-squares extraction of elastic coefficients from ab initio total energy calculations*. Phys. Rev. B 63 (2001), pp. 174103.1–174103.8.
[53] C. Li, B. Wang, R. Wang, H. Wang, and X. Lu, *First-principles study of structural, elastic, electronic, and optical properties of orthorhombic BiGaO3*, Comput. Mater. Sci. 42 (2008), pp. 614–618.
[54] W. Voigt, *Lehrbuch der Kristallphysik* [The textbook of crystal physics], B.G. Teubner, Leipzig und Berlin, 1928.
[55] A. Reuss, *Berechnung der Fliessgrenze von Mischkristallen auf Grund der Plastizitätsbedingung für Einkristalle* [Calculation of the liquid limit of mixed crystals on the basis of the plasticity condition for single crystals], J. Appl. Math. Mech. 9 (1929), pp. 49–58.

[56] R. Hill, *The elastic behaviour of a crystalline aggregate*, Proc. Phys. Soc. A 65 (1952), pp. 349–354.
[57] P. Ravindran, L. Fast, P.A. Korzhavyi, B. Johansson, J. Wills, and O. Eriksson, *Density functional theory for calculation of elastic properties of orthorhombic crystals: Application to TiSi2*, J. Appl. Phys. 84 (1998), pp. 4891–4904.
[58] I.R. Shein and A.L. Ivanovskii, Elastic properties of mono- and polycrystalline hexagonal AlB_2-like diborides of s, p and d metals from first-principles calculations. J. Phys. Condens. Matter 20 (2008), pp. 415218.1–415218.9.
[59] S.F. Pugh, *XCII. Relations between the elastic moduli and the plastic properties of polycrystalline pure metals*. Philos. Mag. Ser. 45 (1954), pp. 823–843.
[60] M. Born and K. Huang, *Dynamical Theory of Crystal Lattices*, Clarendon, Oxford, 1956.
[61] I.R. Shein and A.L. Ivanovskii, *Ab initio study of the elastic and electronic properties of tetragonal Th2NiC2*, Inst. Solid State Chem. 1–8 (2012).
[62] V.V. Bannikov, I.R. Shein, and A.L. Ivanovskii, *Electronic structure, chemical bonding and elastic properties of the first thorium-containing nitride perovskite TaThN3*, Phys. Status Solidi 1 (2007), pp. 89–91.
[63] H. Fu, D. Li, F. Peng, T. Gao, and X. Cheng, *Ab initio calculations of elastic constants and thermodynamic properties of NiAl under high pressures*, Comput. Mater. Sci. 44 (2008), pp. 774–778.
[64] V. Tvergaard and J.W. Hutchinson, *Microcracking in ceramics induced by thermal expansion or elastic anisotropy*, J. Am. Ceram. Soc. 71 (1988), pp. 157–166.
[65] E. Schreiber, O.L. Anderson, and N. Soga, *Elastic Constants and Their Measurements*, McGraw-Hill, New York, NY, 1973.
[66] O.L. Anderson, *A simplified method for calculating the debye temperature from elastic constants*, J. Phys. Chem. Solids 24 (1963), pp. 909–917.
[67] N.V. Smith, *Photoelectron energy spectra and the band structures of the noble metals*, Phys. Rev. B 3 (1971), pp. 1862–1878.
[68] C. Ambrosch-Draxl and J.O. Sofo, *Linear optical properties of solids within the full-potential linearized augmented planewave method*, Comput. Phys. Commun. 175 (2006), pp. 1–14.
[69] M. Fox, *Optical Properties of Solids*, Oxford University Press, New York, NY, 2001.
[70] F. Wooten, *Optical Properties of Solids*, Academic Press, New York, NY, 1972.
[71] M. Maqbool, B. Amin, and I. Ahmad, *Bandgap investigations and the effect of the In and Al concentration on the optical properties of InxAl1-xN*, J. Opt. Soc. Am. B 26 (2009), pp. 2181–2184.
[72] M. Maqbool, M.E. Kordesch, and A. Kayani, *Enhanced cathodoluminescence from an amorphous AlN:holmium phosphor by co-doped Gd+3 for optical devices applications*, J. Opt. Soc. Am. 26 (2009), pp. 998–1001.
[73] S.Zh. Karazhanov, P. Ravindran, A. Kjekshus, H. Fjellvåg, and B.G. Svensson, *Electronic structure and optical properties of ZnX (X=O, S, Se, Te): A density functional study*, Phys. Rev.B 75 (2007), pp. 155104.1–155104.14.
[74] S. Loughin and R.H. French, L.K. De Noyer, W.Y. Ching, and Y.N. XU, *Critical point analysis of the interband transition strength of electrons*, J. Phys. D: Appl. Phys. 29 (1996), pp. 1740–1750. http://iopscience.iop.org/article/10.1088/0022-3727/29/7/009
[75] G. Shwetha and V. Kanchana, *Optical isotropy in structurally anisotropic halide scintillators: Ab initio study*, Phys. Rev. B 86 (2012), pp. 115209.1–115209.8.
[76] S. Azam and A.H. Reshak, *Electronic Structure of 1,3-dicarbomethoxy4,6-benzenedicarboxylic acid: Density functional approach*, Int. J. Electrochem. Sci. 8 (2013), pp. 10359–10375.
[77] A. Togo and I. Tanaka, *First principles phonon calculations in materials science*, Scr. Mater. 108 (2015), pp. 1–5.
[78] S. Baroni, P. Giannozzi, and A. Testa, *Green's-function approach to linear response in solids*, Phys. Rev. Lett. 58 (1987), pp. 1861–1864.
[79] X. Gonze and J.-P. Vigneron, *Density-functional approach to nonlinear-response coefficients of solids*, Phys. Rev. B 39 (1989), pp. 13120–13128.
[80] X. Gonze, D.C. Allan, and M.P. Teter, *Dielectric tensor, effective charges, and phonons in α-quartz by variational density-functional perturbation theory*, Phys. Rev. Lett. 68 (1992), pp. 3603–3606.